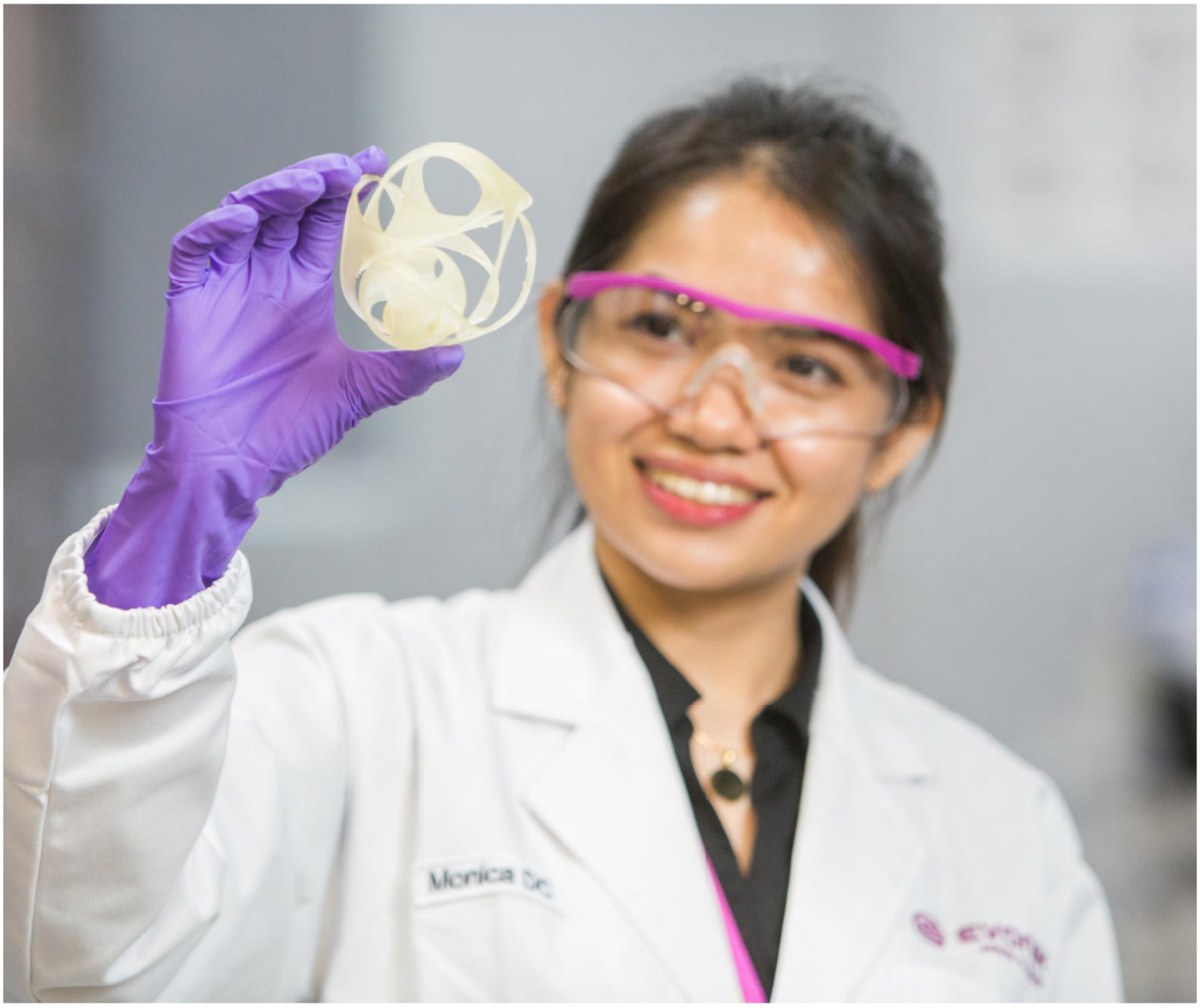

Pushing the boundaries of chemistry? It takes #HumanChemistry

Make your curiosity and talent as a chemist matter to the world with a specialty chemicals leader. Together, we combine cutting-edge science with engineering expertise to create solutions that answer real-world problems. Find out how our approach to technology creates more opportunities for growth, and see what chemistry can do for you at:

evonik.com/career

EVONIK
Leading Beyond Chemistry

ADVANCED FUNCTIONAL MATERIALS
www.afm-journal.de

Continuous Melt-Drawing of Highly Aligned Flexible and Stretchable Semiconducting Microfibers for Organic Electronics

*Yan Zhao, Aristide Gumyusenge, Jiazhi He, Ge Qu, William W. McNutt, Yuan Long, Hongyi Zhang, Libai Huang, Ying Diao, and Jianguo Mei**

A scalable and green approach to manufacture semiconducting microfibers from polymer melts has been demonstrated. The polymer chains are highly aligned along the microfiber's long axis direction and exhibit highly anisotropic optical properties. In addition, the polymer microfibers show good flexibility and stretchability with a yield point around 10% under a reversible stress and can be stretched up to 180% without breaking. These features are desired for future flexible, stretchable, and conformable electronics. The origin of this stretchability is studied with diketopyrrolopyrrole derivatives using different conjugation break spacers and side chains. In addition, stretchable conducting microfibers can be obtained by doping with $FeCl_3$, which are further evaluated as organic conductors and source/drain electrodes in organic field-effect transistors.

1. Introduction

Semiconducting polymers, as a class of complementary and alternative materials to inorganic semiconductors such as silicon, attract a great deal of attention from the aspects of both fundamental and applied research.[1–4] The intense interest lies in the facts that they hold great potential for future low-cost, light-weight, and flexible electronics.[5–7] Semiconducting polymers are typically processed from organic solutions and presented in the form of thin films by various coating/printing techniques. Aside from solution-processed thin films, polymer micro-/nanofibers are also of great interest due to their high-aspect ratio, flexibility in surface functionalities, and superior mechanical performance.[8] These features make semiconducting/conducting polymer micro-/nanofibers attractive for applications in flexible, stretchable, and conformable electronics.[9,10] A variety of processing techniques have been known to prepare conventional polymer fibers, including electrospinning, melt drawing, template synthesis, phase separation, and self-assembly, etc.[8,10–12] Of all the methods, electrospinning and melt drawing are widely adopted for continuous mass manufacturing of polymer fibers.[13] Millions of tons of polymer fibers (i.e., polyethylene and nylon) are produced annually. Although electrospinning and melt drawing of insulating polymer fibers have been widely practiced, they have been hardly applicable to semiconducting polymers. Electrospun semiconducting polymer fibers are often discontinuous and contain lots of beads along the fibers,[14] because semiconducting polymers usually have limited solubility and strong tendency to aggregate that can readily block the nozzles.[15] As a result, semiconducting polymers are usually blended into other insulating polymers for electrospinning.[16] These blended polymer micro-/nanofibers, unfortunately, share similar problems with solution-processed blended thin films (i.e., use of toxic solvents and uncontrolled morphologies) and in general exhibit poor electronic properties in comparison with pure semiconducting polymer thin films. On the other hand, plastic melt "drawing" and alignment have been well documented for over 50 years.[17] However, melt spinning and drawing of semiconducting polymers have seldom been reported because of high melting temperatures or decomposition before melting. This is particularly true for high performance donor–acceptor type semiconducting polymers. At present, it remains a great challenge for scalable fabrication of semiconducting polymer fibers.

Recently, we developed melt-processable semiconducting polymers by introducing nonconjugated flexible linker (conjugation-break spacer, CBS) into the polymer main chain.[18] In this study, by using the diketopyrrolopyrrole (DPP) polymer DPP-C5 (**Figure 1**a), we explore the possibility to manufacture semiconducting microfibers via a continuous melt-drawing process and study the impact of melt drawing on polymer chain alignment. We demonstrate that highly uniform, meters-long polymer microfibers can be obtained from polymer melts. The diameters of the polymer fibers can be tuned from sub-10–100 μm by controlling the processing temperatures and the drawing speeds. Cross-polarized optical microscope (c-POM) and polarized reflectance spectroscopy (PRS) experiments

Dr. Y. Zhao, A. Gumyusenge, J. He, W. W. McNutt, Y. Long, H. Zhang, Prof. L. Huang, Prof. J. Mei
Department of Chemistry
Purdue University
West Lafayette, IN 47907, USA
E-mail: jgmei@purdue.edu
G. Qu, Prof. Y. Diao
Department of Chemical and Biomolecular Engineering
University of Illinois at Urbana–Champaign
Urbana, IL 61801, USA
The ORCID identification number(s) for the author(s) of this article can be found under https://doi.org/10.1002/adfm.201705584.

DOI: 10.1002/adfm.201705584

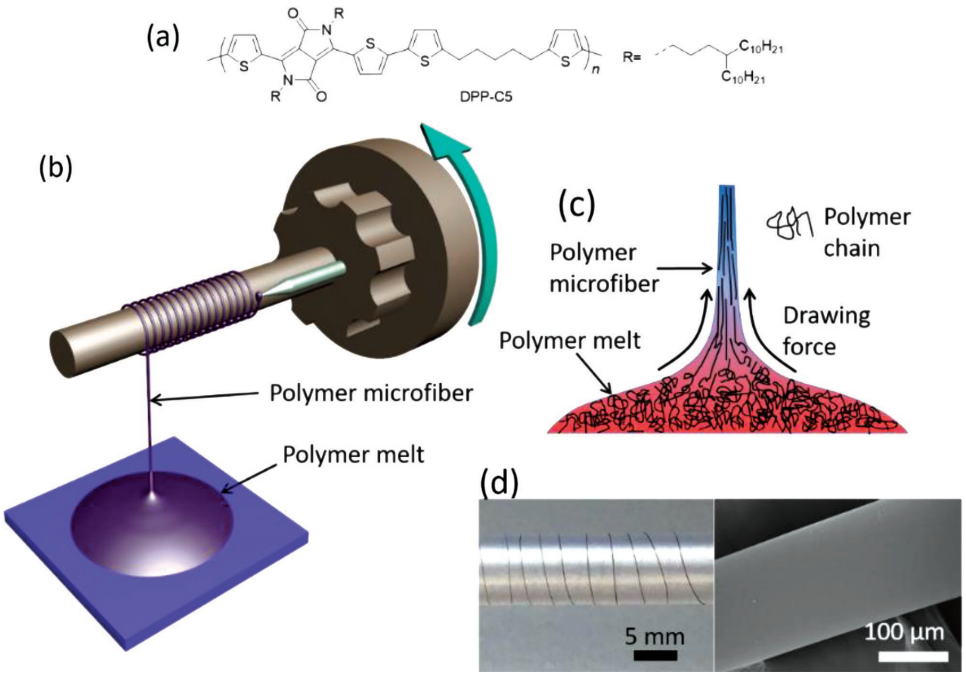

Figure 1. a) Chemical structure of DPP-C5 used in this work. b) Schematic illustration of melt-drawing method using a rotator to collect the polymer microfibers. c) Schematic illustration of the polymer chain alignment during the melt-drawing process. d) Optical image (left, ≈50 μm diameter and 40 cm long) and SEM image of a single polymer microfiber.

indicate the polymer microfibers are highly anisotropic and the polymer chains are aligned along the microfiber's long axis direction with dichroic ratios as high as ten, which is in good agreement with the grazing incidence X-ray diffraction (GIXRD) measurements. The polymer microfibers can be reversibly stretched before the yield point and can sustain up to 180% elongation without breaking. Furthermore, five DPP polymer derivatives have been designed and prepared in order to establish the relationship between molecular structure and mechanical properties. The results show that the CBS length has a big influence on the elastic property, while the side chain has more influence on the degree of elongation. Satisfyingly, flexible and stretchable conducting microfibers can be obtained with iron chloride doping, which are further evaluated as stretchable organic conductors and source/drain electrodes in organic field-effect transistors.

2. Results and Discussion

2.1. Polymer Microfiber Fabrication

The melt-drawing method is briefly described as follows and illustrated in Figure 1b. The solid polymer material was first put on a hot plate and melted at 170 °C. After the polymer became fully liquefied, a needle tip was vertically dipped into the polymer melt and gently pulled up. A fine polymer microfiber was formed immediately after the tip left the surface of polymer melt. The needle was then mounted onto a rotator to collect the polymer microfiber continually (see Video S1 in the Supporting Information). The diameters of polymer microfibers can be controlled by the selection of needle size, pulling speed, and temperature. Small needle size, high temperature (low viscosity), and fast speed will result in thinner microfibers. Through selection of the processing conditions, polymer microfibers with diameters from 5 to 250 μm were obtained (Table S1, Supporting Information). Meters-long polymer microfiber was readily fabricated and showed smooth surface as shown by the scanning electron microscope (SEM) image (Figure 1d). The melt-drawing process and the setup can be found in the Video S1 in the Supporting Information. This process can be easily practiced in an academic laboratory. Conceivably, it is also scalable for mass production of semiconducting polymer microfibers.

2.2. Optical Study of the Polymer Microfibers

With the demonstration of the continuous formation of semiconducting polymer microfiber from melt, we asked what kinds of properties these microfibers exhibit in terms of morphological, optical, electrical, and mechanical properties. To our knowledge, it is a largely unknown question. We first qualitatively characterized the crystallinity and chain alignment of the polymer microfibers via cross-polarized optical microscopy (c-POM). Polymer microfibers with 5–10 μm in diameter and polymer ribbons with 1–2 μm in thickness (fabricated from polymer fibers via pressing) were chosen for the investigation. The c-POM images are displayed in **Figure 2**a–d. Optical birefringence provides a qualitative measure of the extent of global polymer chains alignment in the fibers/ribbons. When the polymer microfibers or ribbons were rotated between the crossed polarizers, the samples switched between dark and bright every 45° (see Video S2 in the Supporting Information).

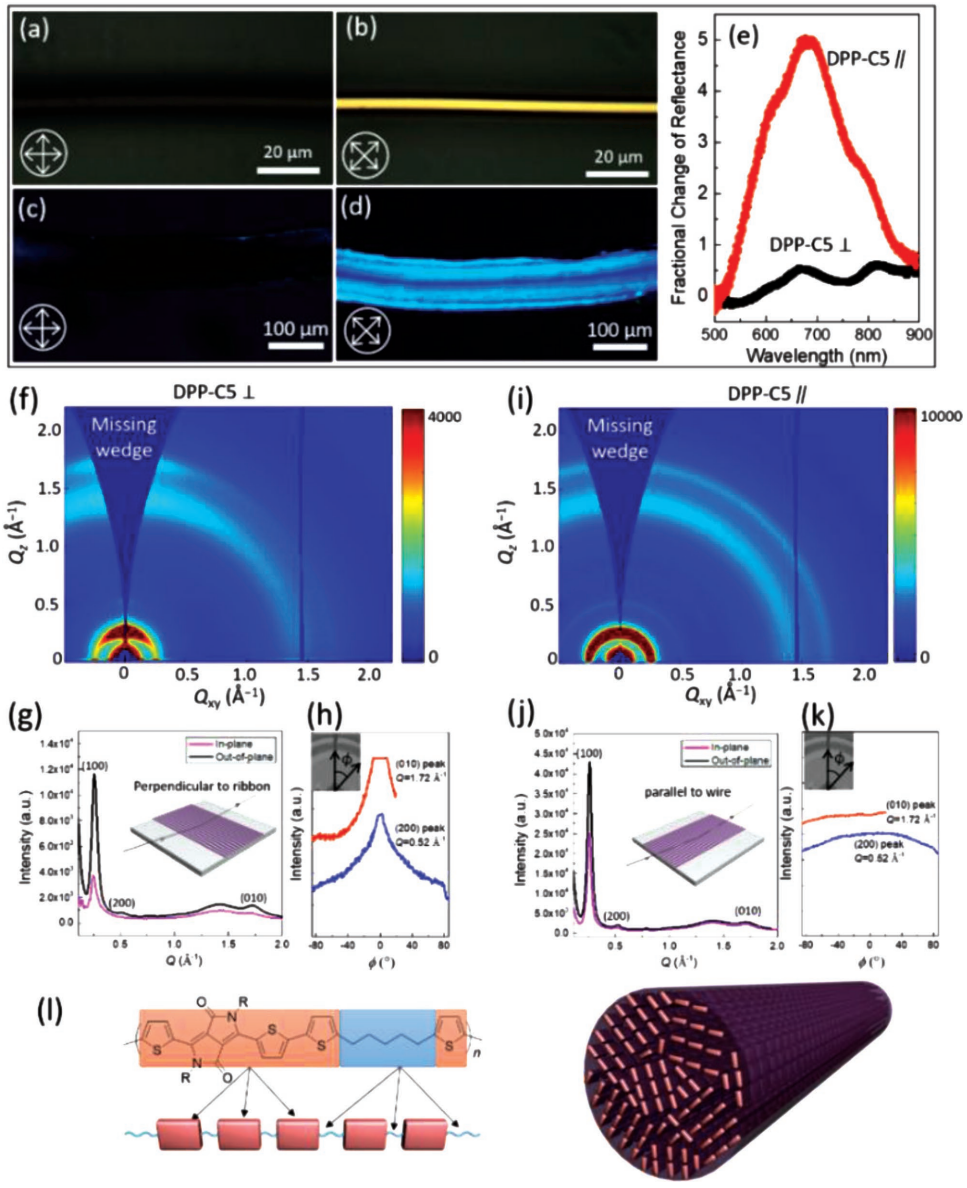

Figure 2. Polymer chain packing characterization. The signs "∥" and "⊥" denote the orientation of the polymer microfiber to the axis of the polarizer or the X-ray beam. a–d) Polarized optical microscope for DPP-C5 a,b) polymer microfiber and c,d) ribbon. The orientation of the crossed-polarizers for each image is shown on the bottom left. e) Polarized microreflection spectroscopy for DPP-C5 ribbon. f) and i), 2D GIXRD patterns for DPP-C5⊥ and DPP-C5∥, respectively. g) and j) are the 1D GIXRD plots obtained from 2D data for DPP-C5⊥, DPP-C5∥, respectively. h) and k) are the azimuthal linecut of the 2D data for DPP-C5⊥ and DPP-C5∥, respectively. l) Schematic illustration of the polymer chains (left) and the chain packing in polymer microfibers.

This optical contrast is originated from birefringence. With nearly 10 μm in diameter, the DPP-C5 microfiber shows a distinct optical contrast (see Figure 2a,b). A total light extinction is observed when the microfiber/ribbon is aligned with either axis of the cross-polarizers, which indicates that the polymer chains are oriented either parallel or perpendicular to the microfiber's long axis direction. It is worth mentioning that the polymer microfibers/ribbons exhibit a uniform color and optical contrast up to centimeter range scale under cross-polarized light (see Figure S1 and Video S1 in the Supporting Information). It suggests that a long range ordering is persistent along the polymer microfibers. This phenomenon has seldom been reported in solution processed semiconducting polymer thin films or fibers.

PRS was further chosen for a quantitative analysis (see Experimental Section in the Supporting Information). The differential reflectance (δ_R) is used here as shown in Figure 2e to quantify the polymer chain alignment. The signs "∥" and "⊥" in Figure 2e denote the orientation of the polymer microfiber/ribbon to the axis of the polarizer. The differential reflectance (δ_R) is defined as

$$\delta_R = \frac{R_{\text{sample}} - R_{\text{substrate}}}{R_{\text{substrate}}} \quad (1)$$

where R_{sample} is the reflectance intensity of sample with substrate and $R_{substrate}$ is the reflectance intensity of bare substrate. For thin film on transparent substrate, the differential reflection is directly related to the absorption coefficient by the following Equation (2)[19]

$$\delta_R = \frac{4}{n_{sub}^2 - 1} A \tag{2}$$

where n_{sub} is the refractive index of substrate and A is the absorption coefficient. According to Equation (2), the differential reflectance is proportional to the absorbance of sample on substrate. For polarized absorbance, the maximum absorption is expected when the transition dipole moments (TDMs) align with the polarizer axis and for DPP based semiconducting polymers, TDMs are usually oriented parallel to the polymer backbone.[20] For DPP-C5 polymer ribbon, the maximum differential reflectance is observed with polymer ribbon parallel to the polarizer axis, which confirms that the polymer chain is oriented parallel to the microfiber long axis direction in agreement with the c-POM results. The degree of polymer chains alignment was further quantified by the dichroic ratio of the peak around 680 nm, using the equation $R = I_{\parallel}/I_{\perp}$, where R is the dichroic ratio and I is the spectrum intensity. The dichroic ratio of DPP-C5 polymer microfiber is 9.6, which is in par with those highly crystalline organic semiconducting films.[21–23]

2D order parameter S is also used to quantify the degree of orientation. The S value can be calculated by the optical dichroic ratio using the following equation[24]

$$S = \frac{R-1}{R+1} = \frac{I_{\parallel} - I_{\perp}}{I_{\parallel} + I_{\perp}} \tag{3}$$

S corresponds to the percentage difference between absorption peak intensities perpendicular and parallel to the alignment direction. For instance, a complete alignment S is equal to unity, whereas for amorphous/disordered material S approaches zero. The calculated S for DPP-C5 is 0.81. It suggests that DPP-C5 polymer chains are highly aligned parallel to the microfiber long axis direction. The degree of the alignment is similar with some of the best-known polymers.[25] Both dichroic ratio R and 2D order parameter S measurements show that the DPP-C5 polymer chains are highly alignment in the microfibers.

2.3. Morphological Study of the Polymer Microfibers

To probe the molecular packing and the origin of anisotropic properties of these melt-drawn polymer microfibers, 2D GIXRD measurement was employed. The single polymer microfiber GIXRD is ideal to study molecular packing, but due to the tiny size of the fibers, it is hard to align the fiber to the X-ray beam and the GIXRD signal is very weak (Figure S5, Supporting Information). Therefore, multiple fibers were used for GIXRD measurement and the microfibers were pressed into ribbons to avoid measurement complication from the smooth and round microfiber surface (Please see the single/multiple fiber GIXRD in Figures S5–S7, Supporting Information). The polymer ribbons were prealigned on a 1.5 × 1.5 cm SiO_2/Si substrate and the X-ray beam was applied either perpendicular or parallel to the same sample with incident angle of 0.14°. The GIXRD patterns are shown in Figure 2f,i. Clear lamellar packing and π–π packing peaks are observed. The calculated packing distances are 24.02 Å for lamellar packing and 3.64 Å for π–π packing. The peak at **Q** vector around 1.4 $Å^{-1}$ is the amorphous peak, which is commonly observed in conjugated polymers.[26] Compared with the thin film packing results in our previous studies,[18] the packing distances in polymer microfibers changed slightly. The lamellar packing distance of DPP-C5 polymer chain is slightly increased from 23.3 Å (thin film) to 24.0 Å (microfiber), and the π–π packing distances of polymer microfibers, on the other hand, are decreased from 3.70 Å (thin film) to 3.64 Å (microfiber). This result suggests that the melt-drawing process results in closer π–π packing distances and larger lamellar distances. It has been previously observed that in molecular organic semiconductors the π–π packing distances can be tuned via solution shearing force.[27] It is reasonable to believe that the extensional flow along the microfiber direction exerts an influence on the polymer chain packing during the melt-drawing process.

For conjugated polymers, the lamellar packing, π–π packing, and polymer chains are orthogonal to each other. In this polymer microfiber, the polymer chains are aligned along the microfiber long axis. Therefore, when the X-ray beam is applied perpendicular to the ribbons/polymer chains, both lamellar packing and π–π packing peaks are expected to only appear along the out-of-plane direction. Figure 2f shows the DPP-C5 ⊥ GIXRD pattern and the result agrees with the expected. 1D GIXRD linecuts for both in-plane and out-of-plane directions are plotted in Figure 2g, and the out-of-plane peak intensities are much stronger than the in-plane intensities. Azimuthal linecut of the lamellar packing and π–π packing peaks is also performed (Figure 2h) to examine the peak intensity changes as function of azimuthal angle φ. The missing data at φ around 0° result from the fact that the true q_z axis is not probed.[28] For the analysis of lamellar packing, (200) peak ($\mathbf{Q} \approx 0.52$ $Å^{-1}$) was chosen, instead of (100 peak). Because the (100) peak is too close to the direct X-ray beam and is thus compounded by the influence of the beam itself. From the Figure 2h, it becomes clear that both (200) and (010) peak intensities are strong along the out-of-plane direction (φ close to 0°), and are very weak along in-plane direction (φ close to ±90°). Both 1D and azimuthal linecut clearly show that both lamellar packing and π–π packing peaks tend to appear in the out-of-plane direction. This once again confirmed the polymer chain alignment along the long axis of the microfibers. For the X-ray parallel to microfibers/ribbons, very uniform diffraction rings were observed for both single microfiber (Figure S5, Supporting Information) and multiple ribbons (Figure 2i). These uniform diffraction rings indicate that although the polymer chains are aligned along the polymer microfiber, there is no preferred orientation for π–π and lamellar packing. Therefore, no anisotropic property can be observed from the GIXRD pattern and thus lead to very similar in-plane and out-of-plane 1D GIXRD curves (Figure 2j). Accordingly, azimuthal linecuts are relatively flat at all ϕ angle (Figure 2k). The proposed packing mode of DPP-C5 polymer chain is shown in Figure 2l.

2.4. Electrical Property of the Polymer Microfibers

Confirmed by the c-POM, PRS, and GIXRD measurements, polymer chains are highly aligned along the microfiber's long axis direction, and their π–π stacking is randomly oriented in the plane perpendicular to the microfiber's long axis (as shown in Figure 2l). Organic field-effect transistors (OFETs) were then fabricated to study the charge transport properties resulting from this uniaxial chain alignment in the polymer microfiber. Devices with microfiber both parallel and perpendicular to the current direction were fabricated and measured. Details about device size, fabrication, and measurement can be found in the Experimental Section in the Supporting Information. More than 10 devices were fabricated for each measurement. Their maximum and average charge carrier mobilities are summarized in Figure S8 (Supporting Information). The direction signs "∥" and "⊥" represent the angle between polymer microfiber (polymer chains) and the channel direction (source/drain current direction), as shown in Figure S8b (Supporting Information). A few intriguing observations were made as follows: (1) DPP-C5⊥ OFETs exhibit a unusally large variation when it comes to charge carrier mobility. (2) DPP-C5⊥gives a maximum mobility of 0.012 $cm^2 Vs^{-1}$, which is nearly tenfolds of the maximum mobility that DPP-C5∥OFETs present (0.0016 $cm^2 Vs^{-1}$). (3) The maximum mobility of DPP-C5⊥ device is even higher than their spin-coated thin film device.

For DPP-C5 polymer, the intrachain charge transport is interrupted by the nonconjugated CBS. Therefore, transport along the π–π packing direction is the only efficient way. This explains why the DPP-C5⊥ devices have better performance than DPP-C5∥ because the DPP-C5∥ devices lack this efficient charge transport pathway. In addition, the DPP-C5 molecules are not all edge-on oriented because the π–π stacking in the microfiber is randomly orientated. Therefore, the charge transport is not that efficient in some face-on-oriented areas (Figure S8e,f, Supporting Information). But for the area with edge-on-oriented DPP-C5 molecules, the closer π–π stacking distance and good orientation are all favored for charge transporting. This explains the large variation of DPP-C5⊥ OFETs and why the maximum mobility of DPP-C5⊥ devices is better than that of the thin-film OFETs. Another possible reason for the large variation of the device performance might from the contact problem. The big size of the microfiber might cause some air gap/bad contact. The measured performances from these devices are underestimated.

2.5. Mechanical Property of the Polymer Microfibers

Flexibility and stretchability are unique features for polymeric semiconductors, which make them especially attractive for soft and conformable/deformable wearable electronics. To evaluate the mechanical properties of the DPP-C5 polymer microfibers, a series of experiments were performed. **Figure 3**a shows a small knot made from an individual polymer microfiber. The radius of curvature is around 30 μm with microfiber diameter around 20 μm. Figure 3b exhibits a knitted architecture from three individual microfibers. A pressed and twisted microribbon under cross-polarized microscopy is also shown in Figure 3c. All three experiments demonstrate the excellent flexibility of the melt-drawn polymer microfibers qualitatively.

The stretchability of polymer microfibers was quantitatively assessed by the stress–strain test with a force gauge and a motorized linear stage. The engineering stress–strain plot is shown in Figure 3d. The initial slope of the stress–strain curve gives a measure of the modulus. It is estimated that the tensile modulus of DPP-C5 polymer microfibers is 0.084 ± 0.021 GPa and the yield point is 9.9 ± 1.5% strain. The polymer microfibers exhibit a reversible deformation before the yield point (see Figure 3e), behaving in an elastic manner. Once stress is removed, the polymer microfibers return to their original shape. The polymer microfibers continue to deform considerably under stress, as revealed by the plateau in the stress–strain curve. In this region, the deformation becomes permanent and the recovery is only partial (Figure S9, Supporting Information). The polymer microfibers show an ultimate elongation up to 180% before breaking (Figure 3d and Figure S9, Supporting Information) with an average fracture strain of 109 ± 31%. Video S3 of the stress–strain experiment can be found in the Supporting Information.

Although some stretchable semiconducting polymers have been reported, most of them are supported by stretchable substrates, usually polydimethylsiloxane.[5] The free-standing stretchable semiconducting polymers have rarely been reported. It has been reported that fully conjugated DPP polymer thin films have relatively low stretchability.[29] With CBS, DPP-C5 exhibits much better stretchability. How the change of chemical structure influences the mechanical properties becomes an interesting question for designing flexible and stretchable semiconducting polymers. DPP derivatives with different conjugation break spacers and side chains (Figure 3f) were studied here for this purpose and the results are shown in Figure 3g,h. Compared with DPP-C5, DPP-C3 with the same side chain but shorter CBS exhibits higher modulus (0.21 ± 0.020 GPa), lower yield point (6.0 ± 0.9% strain), and smaller fracture strain (65 ± 16%). On the other hand, with longer CBS, DPP-C7 exhibits lower modulus (0.027 ± 0.0091 GPa), higher yield point (12.6 ± 1.7% strain), and longer fracture strain (127 ± 27%). Side chains are shown to influence the mechanical properties. With siloxane-terminated side chains, DPP-C5-Si exhibits comparable modulus (0.09 ± 0.033 GPa) and yield point (9.2 ± 1.1%) with DPP-C5, and slightly smaller fracture strain (72.6 ± 11.5%). However, with same CBS but linear C12 as side chain, DPP-C5-*n*-C12 exhibits very poor stretchability (9.7 ± 2.4%), although the yield point (8.2 ± 1.2%) is not changed much.

From all the results obtained, it seems that the CBS length has a large influence on the yield point and the side chain has more influence on the fiber elongation. Comparing DPP-C3, DPP-C5, and DPP-C7, the only difference in molecular structure is the CBS length. Their yield point increased from 6.0%, 9.9% to 12.6%, respectively. On the other hand, with same CBS length but different side chains, DPP-C5, DPP-C5-Si, and DPP-C5-*n*-C12 exhibit similar yield points all around 9%. One possible explanation for these results is that the elastic property (related to the yield point) originates from the flexible nonconjugated CBS, and longer CBS gives higher yield

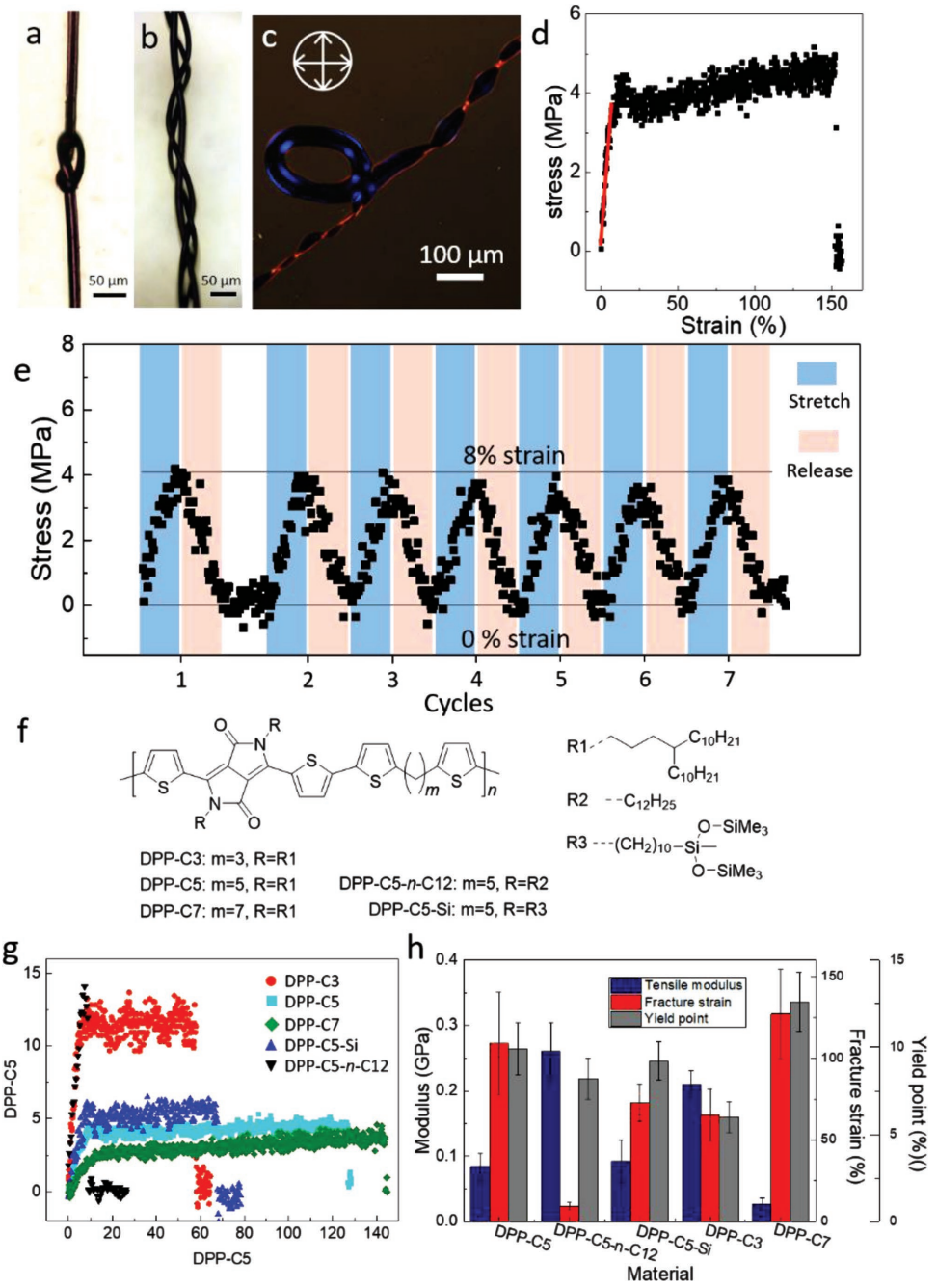

Figure 3. Flexibility and stretchability measurements. a–c) Optical images for the flexible polymer microfibers/ribbons. d) Engineering stress–strain curve for DPP-C5 polymer microfibers. e) Cyclic stretch-release measurement of a representative polymer microfiber. f) Chemical structure of the polymers used for the mechanical study. g) Engineering stress–strain curves for different polymer microfibers and h) their tensile moduli, fracture strains, and yield points calculated from the stress–strain curves.

point. These observations indicate that the side chains have limited influence on the yield point, but play an important role in elongation property. DPP-C5-*n*-C12 with short linear side chain exhibits distinctly different elongation property from all other polymers. The 9.7 ± 2.4% facture strain is much lower than DPP-C5 and DPP-C5-Si. With siloxane-terminated side chains, DPP-C5-Si has much better elongation property, but still not as good as DPP-C5 with long-branched side chains. This result indicates that the longer and branched side chain is favored for elongation property. We understand that the chemical structure also affects the molecular packing and glass transition temperature T_g, and they both have influence on mechanical properties of the fiber. From the current results, however, it is understood that both CBS and side chain can be used to tune the stretchability of semiconducting polymers.

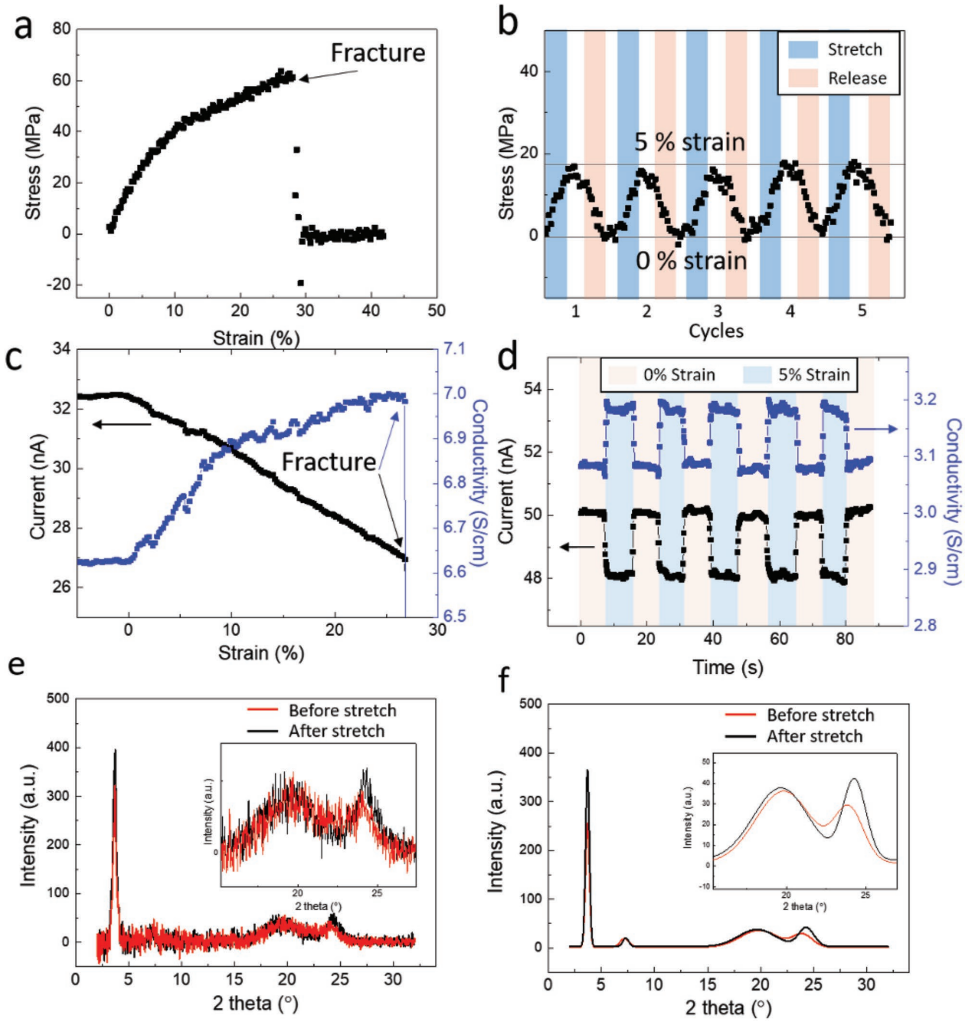

Figure 4. a) The stress–strain curve and b) the cyclic stretch-release measurement of a representative doped DPP-C5 polymer microfiber. c) The current and conductivity as function of strain. d) Conductivity measurement in stretch-release cycles. e) XRD measurement of DPP-C5 microfiber before and after stretching and f) Gauss fitting of the XRD data. Inset figures in (e) and (f) show the π–π peak areas.

2.6. Electrical and Mechanical Properties of the Doped Polymer Microfibers

Our observations of low tensile moduli, high elasticity, and high elongation for DPP-C5 microfibers suggest that these microfibers hold great potential for soft and conformable/deformable electronics (e.g., smart textiles). Therefore, the DPP-C5 polymer microfibers were further doped by $FeCl_3$ to study the electrical and mechanical properties for flexible electronics. The DPP-C5 polymer microfiber was doped in $FeCl_3$ nitromethane solution (100 mg mL^{-1}) for 1 h and dried in vacuum before use. The conductivity of doped DPP-C5 polymer microfiber was measured by both two-probe and four-probe methods (Figure S10, Supporting Information). Both methods give similar results and the average conductivity is 6.2 S cm^{-1}.

The mechanical property is also measured and shown in **Figure** 4a,b. Compared with pure DPP-C5 microfiber, the doped DPP-C5 microfiber exhibits much higher modulus (0.67 ± 0.047 GPa). In addition, instead of reaching a plateau, the stress keeps increasing after the yield point, and the fracture strain is 35.5 ± 10.2%. Although the elongation property of DPP-C5 microfiber decreased after doping, elastic behavior was also observed as shown in cyclic stretch-release measurement (Figure 4b) and the yield point is still around 10% strain. To evaluate the change in conducting behavior under strain, bias voltage was applied and current was measured on the doped microfiber while stretching. The current–strain curve in Figure 4c shows that the current decreased by stretching the doped microfiber. This is explained by the fact the length of the microfiber increased and cross-section area decreased through stretching the polymer microfiber. Both increased length and decreased cross-section area lead to higher resistance, resulting in a smaller current. Interestingly, the estimated conductivity increased as the strain increased. The increase in conductivity is likely resulted from the molecular packing enhancement by the external flow force from stretching. X-ray diffraction (XRD) measurement was carried out on single DPP-C5 microfiber before and after stretching (20% strain, Figure 4e,f and Figure S11, Supporting Information). The results show that after stretching, the lamellar packing and amorphous

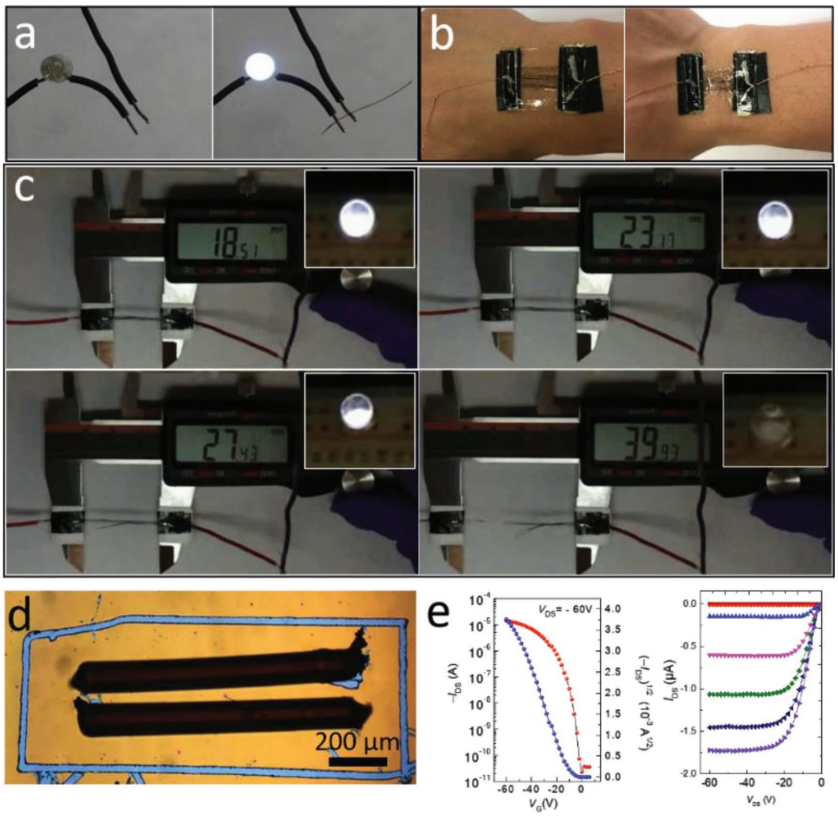

Figure 5. Applications for doped DPP-C5 microfibers. DPP-C5 microfibers as conducting materials: a) light up an LED bulb and b) functioning well with wrist extension and flexion. c) A circuit composed of an LED bulb and doped DPP-C5 microfiber, showing the LED response to the microfiber stretching. d) Doped DPP-C5 microfibers serve as source/drain electrodes for an OFET and e) its transfer and output curves.

peaks positions are almost unchanged, but the π–π packing peak moves to higher two-theta direction, which indicates closer packing distance. The calculated π–π packing distance decreased from 3.71 Å (before) to 3.66 Å (after). This is in good agreement with the GIXRD results discussed above, where a closer π–π packing is resulted from the external flow. In addition, the full width at half-maximum of the π–π packing peaks decreased after stretching (Table S2, Supporting Information), indicating higher ordering. All these observations show that the stretching of polymer microfiber leads to more ordered molecular packing and closer π–π stacking. It is reasonable to believe that better molecular packing leads to better charge transporting and higher conductivity.

With the conductivity and stretchability exhibited above, the polymer microfibers are potential candidates for stretchable electronics. As shown in **Figure 5**a, the 100 μm thick doped DPP-C5 fiber can light up an LED bulb. Figure 5b further shows that the conducting microfibers were functioning well with body motions–extension and flexion of a wrist. The stretchability of these conducting fibers was quantitatively demonstrated with a circuit which is composed of an LED bulb and doped DPP-C5 microfibers as the connecting conducting microwires. The response of LED to stretching was recorded and shown in Video S4 in the Supporting Information. When the polymer microfibers were stretched from their original length (18.51 mm) to 23.17 mm (25% strain), the brightness change of the LED bulb was negligible. The brightness started to decrease rapidly until the microfibers were stretched to 27.43 mm (48% strain), where the microfibers started to break. However, the LED bulb was still on until all microfibers were fractured. This experiment demonstrates the utility of polymer microfibers as stretchable conducting microwires. Furthermore, we tested conducting microfibers as organic electrodes in OFET devices (Figure 5d). Two doped DPP-C5 microfibers were cut into short pieces and arranged parallel on DPP-C5/DPP-C0 blend thin film as source/drain electrodes (Figure S11, Supporting Information). The octadecyltrichlorosilane (OTS) modified 300 nm SiO_2 served as dielectric layer and doped Si as gate electrode. Excellent transfer and output characteristics were obtained, and the charge carrier mobility was around 0.23 cm^2 Vs^{-1}. This performance is comparable to the devices with gold as source/drain electrodes.[30]

3. Conclusion

To summarize, a scalable and green approach to manufacture highly aligned semiconducting microfibers directly from polymer melts has been demonstrated. The microfibers show highly anisotropic optical and electronic properties. They are also soft and stretchable, behaving in an elastic manner under 10% strain and being stretched up to 180% without breaking. The influence of the molecular structure to mechanical property is discussed and the results show that the CBS length has

a large influence on the yield point, and the side chain has more influence on the fiber elongation. These features are highly desired for future flexible, stretchable, and conformable electronics. Applications such as conducting microfibers and electrodes are demonstrated after doped with iron chloride. Currently, we are working on two aspects to carry this study forward. One is to investigate how molecular design affects mechanical property. The other is to establish the relationship among electrical, mechanical, and morphological properties of semiconducting fibers and to elucidate how electrical performance and morphological change are associated with mechanical strain.

Supporting Information

Supporting Information is available from the Wiley Online Library or from the author.

Acknowledgements

The work was mainly supported by the startup fund from Purdue University and the Office of Naval Research Young Investigator Program (ONR YIP), award number N00014-16-1-2551. Y.D. and G.Q. gratefully acknowledge partial support by National Science Foundation, Division of Materials Research under grant number #1641854. This research used resources of the Advanced Photon Source, a U.S. Department of Energy (DOE) Office of Science User Facility operated for the DOE Office of Science by Argonne National Laboratory under Contract No. DE-AC02-06CH11357. The authors thank Dr. Xikang Zhao for providing DPP-C5 material.

Conflict of Interest

The authors declare no conflict of interest.

Keywords

melt drawing, organic electronics, polymer microfibers, semiconducting polymers

Received: September 26, 2017
Published online: November 24, 2017

[1] I. McCulloch, M. Heeney, C. Bailey, K. Genevicius, I. MacDonald, M. Shkunov, D. Sparrowe, S. Tierney, R. Wagner, W. Zhang, M. L. Chabinyc, R. J. Kline, M. D. McGehee, M. F. Toney, *Nat. Mater.* **2006**, *5*, 328.
[2] H. Sirringhaus, *Adv. Mater.* **2014**, *26*, 1319.
[3] Z. B. Henson, K. Mullen, G. C. Bazan, *Nat. Chem.* **2012**, *4*, 699.
[4] C. Wang, H. Dong, W. Hu, Y. Liu, D. Zhu, *Chem. Rev.* **2012**, *112*, 2208.
[5] J. Y. Oh, S. Rondeau-Gagné, Y.-C. Chiu, A. Chortos, F. Lissel, G.-J. N. Wang, B. C. Schroeder, T. Kurosawa, J. Lopez, T. Katsumata, J. Xu, C. Zhu, X. Gu, W.-G. Bae, Y. Kim, L. Jin, J. W. Chung, J. B. H. Tok, Z. Bao, *Nature* **2016**, *539*, 411.
[6] M. L. Hammock, A. Chortos, B. C. K. Tee, J. B. H. Tok, Z. Bao, *Adv. Mater.* **2013**, *25*, 5997.
[7] K. Fukuda, T. Someya, *Adv. Mater.* **2017**, *29*, 1602736.
[8] Z. M. Huang, Y. Z. Zhang, M. Kotaki, S. Ramakrishna, *Compos. Sci. Technol.* **2003**, *63*, 2223.
[9] J. Xu, S. Wang, G.-J. N. Wang, C. Zhu, S. Luo, L. Jin, X. Gu, S. Chen, V. R. Feig, J. W. F. To, S. Rondeau-Gagné, J. Park, B. C. Schroeder, C. Lu, J. Y. Oh, Y. Wang, Y.-H. Kim, H. Yan, R. Sinclair, D. Zhou, G. Xue, B. Murmann, C. Linder, W. Cai, J. B.-H. Tok, J. W. Chung, Z. Bao, *Science* **2017**, *355*, 59.
[10] S. H. Wang, M. Kappl, I. Liebewirth, M. Muller, K. Kirchhoff, W. Pisula, K. Mullen, *Adv. Mater.* **2012**, *24*, 417.
[11] Y. S. Zhao, H. Fu, A. Peng, Y. Ma, D. Xiao, J. Yao, *Adv. Mater.* **2008**, *20*, 2859.
[12] C. Schonenberger, B. M. I. van der Zande, L. G. J. Fokkink, M. Henny, C. Schmid, M. Kruger, A. Bachtold, R. Huber, H. Birk, U. Staufer, *J. Phys. Chem. B* **1997**, *101*, 5497.
[13] N. Bhardwaj, S. C. Kundu, *Biotechnol. Adv.* **2010**, *28*, 325.
[14] A. Luzio, E. V. Canesi, C. Bertarelli, M. Caironi, *Materials* **2014**, *7*, 906.
[15] S. Lee, G. D. Moon, U. Jeong, *J. Mater. Chem.* **2009**, *19*, 743.
[16] E. V. Canesi, A. Luzio, B. Saglio, A. Bianco, M. Caironi, C. Bertarelli, *ACS Macro Lett.* **2012**, *1*, 366.
[17] F. J. Baltacalleja, A. Peterlin, *J. Mater. Sci.* **1969**, *4*, 722.
[18] Y. Zhao, X. Zhao, M. Roders, A. Gumyusenge, A. L. Ayzner, J. Mei, *Adv. Mater.* **2017**, *29*, 1605056.
[19] K. F. Mak, M. Y. Sfeir, Y. Wu, C. H. Lui, J. A. Misewich, T. F. Heinz, *Phys. Rev. Lett.* **2008**, *101*, 196405.
[20] D. M. DeLongchamp, R. J. Kline, Y. Jung, D. S. Germack, E. K. Lin, A. J. Moad, L. J. Richter, M. F. Toney, M. Heeney, I. McCulloch, *ACS Nano* **2009**, *3*, 780.
[21] H. Sirringhaus, R. J. Wilson, R. H. Friend, M. Inbasekaran, W. Wu, E. P. Woo, M. Grell, D. D. C. Bradley, *Appl. Phys. Lett.* **2000**, *77*, 406.
[22] L. Shaw, P. Hayoz, Y. Diao, J. A. Reinspach, J. W. F. To, M. F. Toney, R. T. Weitz, Z. N. Bao, *ACS Appl. Mater. Interfaces* **2016**, *8*, 9285.
[23] S. Schott, E. Gann, L. Thomsen, S. H. Jung, J. K. Lee, C. R. McNeill, H. Sirringhaus, *Adv. Mater.* **2015**, *27*, 7356.
[24] B. O'Connor, R. J. Kline, B. R. Conrad, L. J. Richter, D. Gundlach, M. F. Toney, D. M. DeLongchamp, *Adv. Funct. Mater.* **2011**, *21*, 3697.
[25] Z. Zheng, K.-H. Yim, M. S. M. Saifullah, M. E. Welland, R. H. Friend, J.-S. Kim, W. T. S. Huck, *Nano Lett.* **2007**, *7*, 987.
[26] J. D. Yuen, F. Wudl, *Energy Environ. Sci.* **2013**, *6*, 392.
[27] G. Giri, E. Verploegen, S. C. B. Mannsfeld, S. Atahan-Evrenk, D. H. Kim, S. Y. Lee, H. A. Becerril, A. Aspuru-Guzik, M. F. Toney, Z. Bao, *Nature* **2011**, *480*, 504.
[28] Z. Jiang, *J. Appl. Crystallogr.* **2015**, *48*, 917.
[29] B. Roth, S. Savagatrup, N. V. de los Santos, O. Hagemann, J. E. Carle, M. Helgesen, F. Livi, E. Bundgaard, R. R. Sondergaard, F. C. Krebs, D. J. Lipomi, *Chem. Mater.* **2016**, *28*, 2363.
[30] X. Zhao, Y. Zhao, Q. Ge, K. Butrouna, Y. Diao, K. R. Graham, J. Mei, *Macromolecules* **2016**, *49*, 2601.